PCP
PLANT & CELL PHYSIOLOGY

Rapid Paper

Anthriscus sylvestris Deoxypodophyllotoxin Synthase Involved in the Podophyllotoxin Biosynthesis

Keisuke Kobayashi[1], Masaomi Yamamura[1,2], Bunzo Mikami[1], Akira Shiraishi[3], Masato Kumatani[1], Honoo Satake[3], Eiichiro Ono[4] and Toshiaki Umezawa[1,*]

[1]Research Institute for Sustainable Humanosphere, Kyoto University, Gokasho, Uji, Kyoto, 611-0011 Japan
[2]Faculty of Bioscience and Bioindustry, Tokushima University, 2-1, Minami-josanjima-cho, Tokushima, 770-8502 Japan
[3]Bioorganic Research Institute, Suntory Foundation for Life Sciences, 8-1-1 Seikadai, Seika-cho, Soraku-gun, Kyoto, 619-0284 Japan
[4]Research Institute, Suntory Global Innovation Center Ltd., 8-1-1 Seikadai, Seika-cho, Soraku-gun, Kyoto, 619-0284 Japan

*Corresponding author: E-mail, tumezawa@rish.kyoto-u.ac.jp

(Received 25 December 2022; Accepted 14 September 2023)

Tetrahydrofuran ring formation from dibenzylbutyrolactone lignans is a key step in the biosynthesis of aryltetralin lignans including deoxypodophyllotoxin and podophyllotoxin. Previously, Fe(II)- and 2-oxoglutarate-dependent dioxygenase (2-ODD) from *Podophyllum hexandrum* (Himalayan mayapple, Berberidaceae) was found to catalyze the cyclization of a dibenzylbutyrolactone lignan, yatein, to give deoxypodophyllotoxin and designated as deoxypodophyllotoxin synthase (DPS). Recently, we reported that the biosynthesis of deoxypodophyllotoxin and podophyllotoxin evolved in a lineage-specific manner in phylogenetically unrelated plant species such as *P. hexandrum* and *Anthriscus sylvestris* (cow parsley, Apiaceae). Therefore, a comprehensive understanding of the characteristics of DPSs that catalyze the cyclization of yatein to deoxypodophyllotoxin in various plant species is important. However, for plant species other than *P. hexandrum*, the isolation of the DPS enzyme gene and the type of the enzyme, e.g. whether it is 2-ODD or another type of enzyme such as cytochrome P-450, have not been reported. In this study, we report the identification and characterization of *A. sylvestris* DPS (AsDPS). Phylogenetic analysis showed that AsDPS belonged to the 2-ODD superfamily and shared moderate amino acid sequence identity (40.8%) with *P. hexandrum* deoxypodophyllotoxin synthase (PhDPS). Recombinant protein assay indicated that AsDPS and PhDPS differ in terms of the selectivity of substrate enantiomers. Protein modeling using AlphaFold2 and site-directed mutagenesis indicated that the Tyr305 residue of AsDPS probably contributes to substrate recognition. This study advances our understanding of the podophyllotoxin biosynthetic pathway in *A. sylvestris* and provides new insight into 2-ODD involved in plant secondary (specialized) metabolism.

Keywords: 2-Oxoglutarate-dependent dioxygenase • *Anthriscus sylvestris* • Deoxypodophyllotoxin synthase • Lignan • Podophyllotoxin • Yatein

Introduction

Lignans are phenylpropanoid dimers where the monomers are linked by central (C8) carbon atoms of their propyl side chains (Umezawa 2003a, 2003b). They constitute abundant classes of secondary (specialized) metabolites and are widely distributed in the plant kingdom (Umezawa 2003a, 2003b). Lignans are classified into eight subgroups based on their skeletal structure: furofuran, furan, dibenzylbutane, dibenzylbutyrolactone, aryltetralin, arylnaphthalene, dibenzocyclooctadiene and dibenzylbutyrolactol (Umezawa 2003a).

Some lignans have various biological activities, including antioxidative, antiviral and antitumor effects (MacRae and Towers 1984, Saleem et al. 2005, Satake et al. 2015, Zálešák et al. 2019). For example, arctigenin has several beneficial effects on human health, including anti-inflammatory, anti-influenza virus and neuroprotective activities (Jang et al. 2002, Hayashi et al. 2010, Hyam et al. 2013, Gao et al. 2018), while sesamin has biological activities such as anti-inflammatory activity, inhibition of cholesterol absorption and protection against oxidative DNA damage in the liver (Hirose et al. 1991, Akimoto et al. 1993, Liu et al. 2013, Majdalawieh et al. 2022). An antitumor aryltetralin lignan, podophyllotoxin, prevents cell growth by inhibiting the polymerization of tubulin and has been used in a therapeutic cream for treating human papillomavirus infection (Kollipara et al. 2015, Saitoh et al. 2008). This lignan is also an important plant natural product as a precursor for chemical synthesis of the topoisomerase II inhibitor etoposide (Stähelin and von Wartburg 1991, Canel et al. 2000, Gordaliza et al. 2004, Motyka et al. 2023), which is on the World Health Organization's list of essential medicines used clinically to treat various cancers, including lymphoma, testicular cancer and lung cancer (Hande 1998). However, the primary plant resource for podophyllotoxin production, *Podophyllum hexandrum* (*Sinopodophyllum hexandrum*, Himalayan mayapple), is an endangered species, and thus, shortages in the supply of etoposide have occurred several times in the past few decades (Canel et al. 2000, Lata et al. 2009, Guerram et al. 2012, Li and Cimino 2020). Meanwhile, the

Plant Cell Physiol. 64(12): 1436–1448 (2023) doi:https://doi.org/10.1093/pcp/pcad103, Advance Access publication on 25 October 2023, available online at https://academic.oup.com/pcp
© The Author(s) 2023. Published by Oxford University Press on behalf of Japanese Society of Plant Physiologists. All rights reserved.
For permissions, please e-mail: journals.permissions@oup.com

Downloaded from https://academic.oup.com/pcp/article/64/12/1436/7329445 by guest on 22 May 2025

chemical synthesis of podophyllotoxin is costly and impractical. Therefore, much attention has been focused on the biotechnological production of podophyllotoxin and related compounds. To achieve this, the mechanisms behind the biosynthesis of these lignans should be elucidated and the genes encoding the enzymes involved need to be identified. This knowledge could then be applied to establishing biotechnological approaches to produce these lignans by reconstructing the biosynthetic pathway in heterologous expression systems such as *Escherichia coli*, yeast and *Nicotiana benthamiana* (Lau and Sattely 2015, Cravens et al. 2019, Srinivasan and Smolke 2020, Liu et al. 2021).

In addition to *Podophyllum* spp., various plant species produce podophyllotoxin and related lignans, which are sporadically distributed in plant phylogeny, including eudicot species such as *Anthriscus* spp. and *Linum* spp., basal angiosperm species such as *Hernandia* spp. and gymnosperms such as *Thujopsis* spp. (Sackett 1993, Umezawa 2003a, 2003b, Lata et al. 2009, Biswas et al. 2020). Among them, *Anthriscus sylvestris* is a good source of yatein and deoxypodophyllotoxin, which are biosynthetic precursors of podophyllotoxin (Van Uden et al. 1997, Sakakibara et al. 2003, Umezawa 2003a, 2003b, Suzuki and Umezawa 2007, Hendrawati et al. 2011, Orčić et al. 2021). Hence, this plant has been used by our group for studies of podophyllotoxin biosynthesis. Sakakibara et al. (2003) proposed the two biosynthetic pathways shown in **Fig. 1**; one is the pathway from matairesinol to yatein via thujaplicatin, 5-*O*-methylthujaplicatin and 4,5-*O*,*O*-dimethylthujaplicatin, while the other is the shunt from matairesinol to bursehernin via pluviatolide. They also concluded that the latter shunt did not lead to yatein (**Fig. 1**). Ragamustari et al. (2013) identified a gene from *A. sylvestris* that encodes an *O*-methyltransferase (OMT). This enzyme catalyzes the regioselective methylation of thujaplicatin to produce 5-*O*-methylthujaplicatin, which was designated as *A. sylvestris* thujaplicatin OMT (AsTJOMT). Later, Yamamura et al. (2023) isolated a gene encoding another *A. sylvestris* OMT [seconoryatein OMT (SNYOMT)] that catalyzes the next step in the pathway, which is the methylation of 5-*O*-methylthujaplicatin to give rise to 4,5-*O*,*O*-dimethylthujaplicatin.

Marques et al. (2013) identified genes encoding the cytochrome P-450 (CYP) enzyme that catalyzes pluviatolide formation from matairesinol in *Podophyllum peltatum* and *P. hexandrum* (**Fig. 1**), and Lau and Sattely (2015) identified a series of genes involved in the biosynthesis of 4-*O*-demethylpodophyllotoxin in *P. hexandrum* (**Fig. 1**). The *P. hexandrum* pathway involves yatein as a pivotal intermediate, as in *A. sylvestris*. In sharp contrast to the *A. sylvestris* pathway, however, the pluviatolide/bursehernin shunt leads to yatein in *P. hexandrum* (**Fig. 1**). The *P. hexandrum* pathway involves two OMTs, which exhibited only low amino acid sequence identity to the AsOMTs and were assigned to completely different from those of the AsOMTs.

Taking these findings together, the biosynthetic pathways from matairesinol to yatein differ among phylogenetically unrelated plant species, and the ability to synthesize podophyllotoxin has been acquired by convergent evolution in each plant lineage (**Fig. 1**) (Umezawa et al. 2019, Yamamura et al. 2023). Meanwhile, the conversion of yatein to afford deoxypodophyllotoxin appears to operate in both *Podophyllum* and *Anthriscus* (**Fig. 1**). Sakakibara et al. (2003) demonstrated the

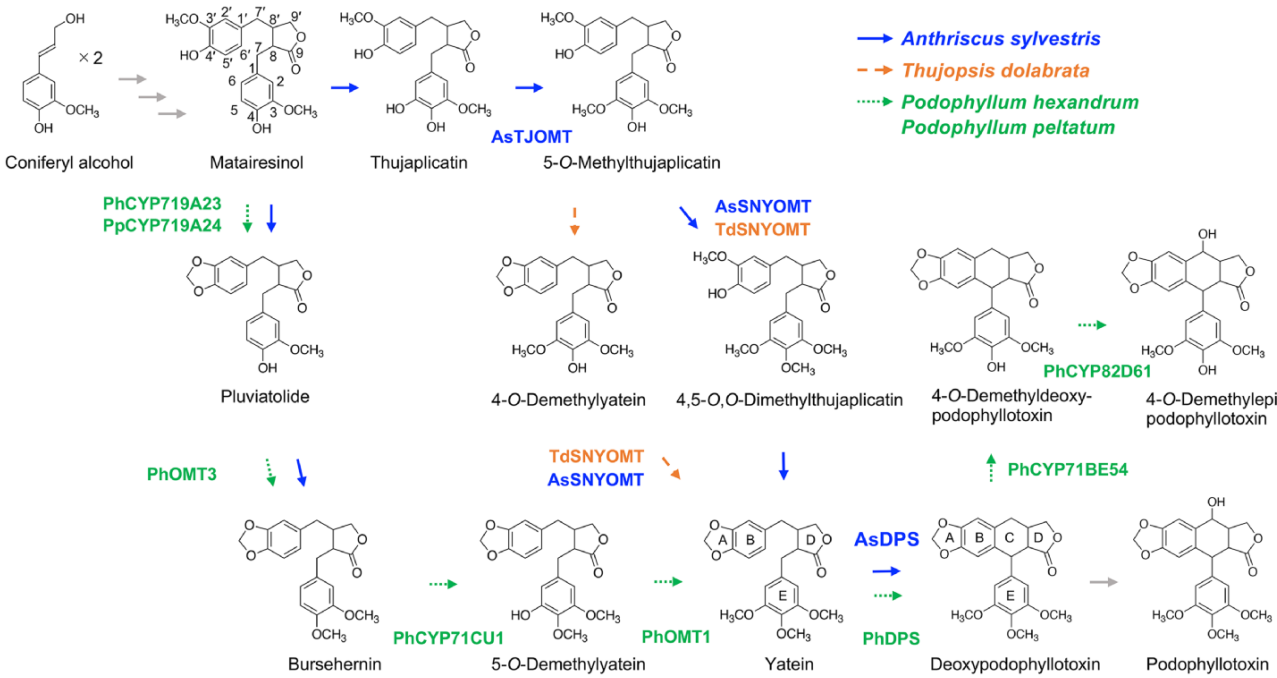


Fig. 1 The proposed biosynthetic pathways for podophyollotoxin in several plants. Blue: *A. sylvestris*, orange: *T. dolabrata* and green: *P. hexandrum* and *P. peltatum*.

Downloaded from https://academic.oup.com/pcp/article/64/12/1436/7329445 by guest on 22 May 2025

in vivo conversion of stable-isotope-labeled yatein into deoxypodophyllotoxin in *A. sylvestris*, while Lau and Sattely (2015) identified from *P. hexandrum* a gene encoding Fe(II)- and 2-oxoglutarate-dependent dioxygenase (2-ODD) that catalyzes the cyclization of yatein to deoxypodophyllotoxin. Recently, Tang et al. (2022) proposed a mechanism for the conversion of yatein into deoxypodophyllotoxin catalyzed by the 2-ODD, *P. hexandrum* deoxypodophyllotoxin synthase (PhDPS). Given that the biosynthesis of the lignans shows a signature of convergent evolution in each plant species, CYP-catalyzed cyclization of yatein to give deoxypodophyllotoxin still appeared possible in *A. sylvestris*, as in flavone synthesis, which can be catalyzed by both 2-ODDs [flavone synthase I (FNS I)] (Kawai et al. 2014) and CYPs [flavone synthase II (FNS II)] (Lam et al. 2021). In addition, if *A. sylvestris* deoxypodophyllotoxin synthase (AsDPS) is a 2-ODD enzyme, it would be intriguing to compare the characteristics of PhDPS (Tang et al. 2022) and *Anthriscus* enzymes that are involved in deoxypodophyllotoxin formation, taking the convergent evolution signature into account.

Herein, we report that *A. sylvestris* 2-ODD exhibits a deoxypodophyllotoxin synthase (DPS) activity, catalyzing the cyclization of yatein to deoxypodophyllotoxin. Phylogenetic analysis indicated that AsDPS and PhDPS share moderate amino acid sequence identity (40.8%), while they exhibit different selectivity in terms of substrate enantiomers. In addition, we suggest that the aromatic ring of Tyr305 of AsDPS is involved in substrate recognition.

Results

Screening of candidate genes involved in the cyclization of yatein

To screen candidate genes involved in the cyclization of yatein, we conducted tBLASTx search on our *A. sylvestris* RNA-seq data (367,585 contigs) (Yamamura et al. 2023) using *PhDPS* as a query (Lau and Sattely 2015). Nine putative *2-ODD* with higher identity were selected. The *2-ODD* contigs were referred to as *As2-ODD-1*–*As2-ODD-9* in decreasing order of expression level [fragments per kilobase of exon per million mapped reads (FPKM) values] (**Fig. 2**). Next, the correlation of the FPKM values between each *As2-ODD* contig and *AsSNYOMT* (Yamamura et al. 2023) was calculated. Three *As2-ODD* contigs (*As2-ODD-1*, *As2-ODD-2* and *As2-ODD-3*) exhibited higher FPKM values (640.39, 525.28 and 516.28, respectively) and co-expression efficiency (0.85, 0.84 and 0.84, respectively) than the other contigs (**Fig. 2**).

Then, these three contigs were subjected to a DPS activity assay with the corresponding recombinant proteins. Because the 5′- and 3′-end sequences of the coding sequence (CDS) were the same for *As2-ODD-2* and *As2-ODD-3*, we employed the same forward and reverse primer set for polymerase chain reaction (PCR) amplification of the CDSs of the two contigs (**Supplementary Table S1**). The CDSs for *As2-ODD-1* and *As2-ODD-2* were amplified by PCR, while the *As2-ODD-3* sequence was not amplified; therefore, we further evaluated only *As2-ODD-1* and *As2-ODD-2*, the deduced protein sequences of which shared 41.1% and 40.8% amino acid sequence identity with PhDPS, respectively. As2-ODD-1 and As2-ODD-2 shared 74.5% amino acid sequence identity with each other.

As2-ODD-2 catalyzed cyclization of yatein

To examine whether As2-ODD-1 and As2-ODD-2 can catalyze the cyclization of yatein to deoxypodophyllotoxin, we expressed recombinant (rec) proteins using *E. coli*. We first used pET-30a as an expression vector for both *As2-ODD-1* and *As2-ODD-2*. A soluble protein with the deduced molecular mass of As2-ODD-2 was obtained, while this was not achieved for As2-ODD-1. Other vectors, pET-15b, pET-23a, pCold1 and pCold2, also did not afford a soluble protein corresponding to As2-ODD-1. We next attempted to use the pCold TF DNA vector, which was co-expressed with the TF tag working as support for the solubilization and folding of the recAs2-ODD-1 protein. This system afforded the corresponding soluble protein. Therefore, recAs2-ODD-1 and recAs2-ODD-2 were subjected to deoxypodophyllotoxin-forming enzyme assay, in accordance with the assay condition [10 mM 2-oxoglutaric acid (2OG) and 10 mM ascorbic acid] with PhDPS (Lau and Sattely 2015). Gas chromatography–mass spectrometry (GC-MS) [selected-ion monitoring (SIM) mode] analysis of the As2-ODD-2 assay products suggested the formation of trace

FPKM Low High

	A			B		C			D					Correlation efficiency	FPKM MAX
	Stem	Leaf	All	Stem	Leaf	Stem	Leaf	Root	Stem	Leaf	Petiole	Flower	Peduncle		
AsSNYOMT	57.12	22.94	40.71	103.85	27.61	67.30	13.47	231.02	24.76	23.21	98.99	13.11	23.79	1.00	231.02
As2-ODD-1	285.04	101.96	317.24	586.00	144.71	56.42	26.14	640.39	76.82	129.52	326.49	7.52	9.00	0.85	640.39
As2-ODD-2	235.23	76.58	246.91	525.28	114.94	45.26	20.38	520.19	60.79	100.26	274.25	5.66	6.65	0.84	525.28
As2-ODD-3	231.20	75.27	242.68	516.28	112.97	44.48	20.03	511.28	59.75	98.54	269.55	5.56	6.53	0.84	516.28
As2-ODD-4	3.22	15.51	1.28	1.32	1.57	1.73	2.70	3.18	2.20	1.13	1.35	1.44	0.30	-0.08	15.51
As2-ODD-5	1.11	0.03	0.75	3.00	0.40	1.81	0.34	1.07	0.65	0.20	2.65	1.08	2.64	0.34	3.00
As2-ODD-6	0.03	1.07	1.92	0.03	0.47	0.00	1.17	0.00	0.00	2.77	0.07	1.06	0.03	-0.42	2.77
As2-ODD-7	0.03	1.07	1.92	0.03	0.47	0.00	1.17	0.00	0.00	2.77	0.07	1.06	0.03	-0.42	2.77
As2-ODD-8	0.03	0.00	0.11	0.34	0.00	0.00	0.00	0.04	0.42	0.18	0.00	1.44	0.21	-0.25	1.44
As2-ODD-9	0.03	0.00	0.11	0.33	0.00	0.00	0.00	0.04	0.41	0.17	0.00	1.38	0.20	-0.25	1.38

Fig. 2 FPKM values of candidate genes and *AsSNYOMT* in various organs of *A. sylvestris* (plant height: A <5 cm, B ca. 10 cm, C 15–20 cm and D >30 cm) and correlation with the expression pattern of *AsSNYOMT*.

Downloaded from https://academic.oup.com/pcp/article/64/12/1436/7329445 by guest on 22 May 2025

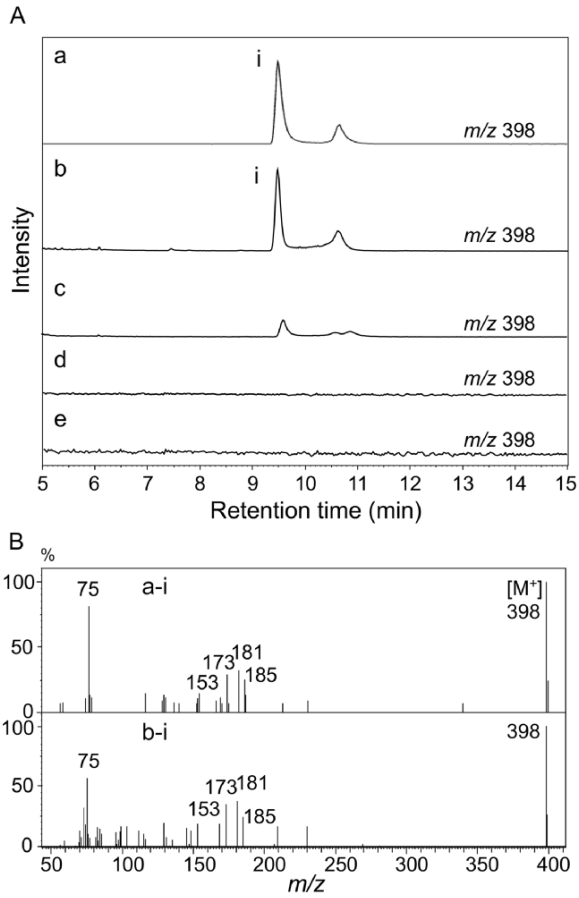


Fig. 3 The GC-MS analysis of authentic lignans and reaction products obtained following the incubation of lignans with recAs2-ODDs (TMS ethers). (A) SIM chromatograms of authentic deoxypodophyllotoxin and each enzyme assay product. a: Authentic (−)-deoxypodophyllotoxin, b: a product formed following the incubation of (±)-yateins with recAs2-ODD-2 in the presence of 0.1 mM 2OG and 0.1 mM ascorbic acid, c: a product formed following the incubation of (±)-yateins with recAs2-ODD-2 in the presence of 10 mM 2OG and 10 mM ascorbic acid, d: no product detected following the incubation of (±)-yateins with recAs2-ODD-1 in the presence of 0.1 mM 2OG and 0.1 mM ascorbic acid and e: negative control using heat-denatured recAs2-ODD-2. (B) Mass spectra of authentic deoxypodophyllotoxin and the enzyme assay product. a-i: The peak i of authentic (−)-deoxypodophyllotoxin (A a), b-i: the peak i of a product (A b) formed following the incubation of (±)-yateins with recAs2-ODD-2 in the presence of 0.1 mM 2OG and 0.1 mM ascorbic acid.

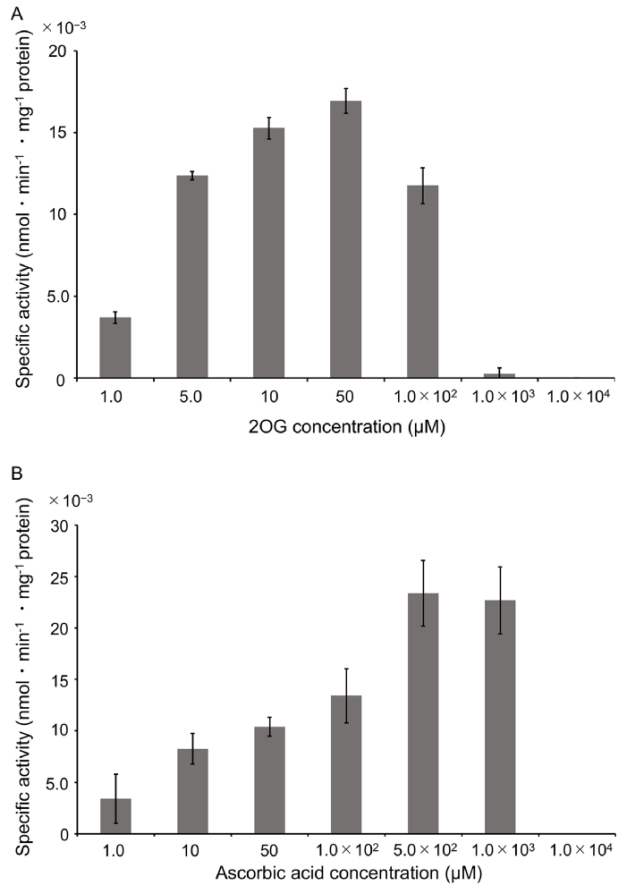


Fig. 4 Effects of co-substrate concentration on the specific activity of recAsDPS. (A) 2OG. (B) Ascorbic acid. The error bars represent the standard deviation of technical replicates ($n = 3$).

amounts of deoxypodophyllotoxin from (±)-yateins (**Fig. 3A c**). Next, under assay conditions in which the concentration of 2OG and ascorbic acid was reduced by two orders of magnitude, recAs2-ODD-2 showed high activity to produce deoxypodophyllotoxin, which was identified by comparing the mass spectrum and retention time with those of an authentic sample (**Fig. 3A b** and **3B b-i**). Meanwhile, crude recAs2-ODD-1 did not show activity even under the modified condition (**Fig. 3A d**). Hereinafter, As2-ODD-2 is referred to as AsDPS.

Next, the effects of the concentrations of co-factors, 2OG and ascorbic acid, on the enzyme activity of purified recAsDPS were examined. As shown in **Fig. 4**, the activity showed marked concentration dependence. AsDPS activity increased as 2OG concentration increased to 50 μM and then decreased with higher 2OG concentration, and no enzyme activity was detected at 10 mM 2OG (**Fig. 4A**). As the ascorbic acid concentration increased up to 500 μM, the activity increased, while it diminished at 10 mM ascorbic acid (**Fig. 4B**). This showed that recAsDPS is inhibited by high concentrations of 2OG and ascorbic acid. Therefore, the concentrations of 50 μM 2OG and 500 μM ascorbic acid were used for the biochemical characterization of recAsDPS. Meanwhile, recAs2-ODD-1 did not show activity under any of the co-factor concentrations employed. As for $FeSO_4$ concentration, there was no significant difference in the enzyme activity in the range of 0.5–50 mM.

Biochemical characterization of AsDPS

Purified recAsDPS (**Supplementary Fig. S1**) showed an optimum temperature of 20°C and an optimum pH of 7.0 (50 mM Tris-HCl) (**Supplementary Fig. S2**). RecAsDPS exhibited V_{max} of 0.72 ± 0.06 nmol· min^{-1}· mg^{-1} protein, K_m of $11.32 \pm$

Downloaded from https://academic.oup.com/pcp/article/64/12/1436/7329445 by guest on 22 May 2025

Table 1 Specific activity of recAsDPS_WT and recAsDPS mutants (AsDPS_Y305L, AsDPS_Y305F and AsDPS_Y305A) toward (±)-yateins-d_6, (−)-yatein-d_6 and (+)-yatein-d_6

	Specific activity (nmol· min^{-1}· mg^{-1} protein)		
	(±)-Yateins-d_6	(−)-Yatein-d_6	(+)-Yatein-d_6
recAsDPS_WT	0.29 ± 0.10	0.59 ± 0.08	0
recAs-DPS_Y305L	0	0	0
recAs-DPS_Y305F	0.24 ± 0.02	0.62 ± 0.16	0
recAs-DPS_Y305A	0	0	0

The plus/minus represents the standard deviation of technical replicates ($n = 3$).

Table 2 Kinetic data for recAsDPS_WT and recAsDPS_Y305F

Enzyme	recAsDPS_WT	
Substrate	(±)-Yateins-d_6	(−)-Yatein-d_6
K_m (μM)	11.32 ± 2.56	22.57 ± 0.88
V_{max} (nmol· min^{-1}· mg^{-1} protein)	0.72 ± 0.06	3.00 ± 0.05
k_{cat} (min^{-1})	$2.71 \times 10^{-2} \pm 2.13 \times 10^{-3}$	$0.11 \pm 1.76 \times 10^{-3}$
k_{cat}/K_m (μM^{-1}· min^{-1})	$2.49 \times 10^{-3} \pm 4.33 \times 10^{-4}$	$5.01 \times 10^{-3} \pm 1.15 \times 10^{-4}$
Enzyme	recAsDPS_Y305F	
Substrate	(±)-Yateins-d_6	(−)-Yatein-d_6
K_m (μM)	19.17 ± 4.8	18.12 ± 1.72
V_{max} (nmol· min^{-1}· mg^{-1} protein)	1.22 ± 0.13	2.35 ± 0.17
k_{cat} (min^{-1})	$4.61 \times 10^{-2} \pm 5.00 \times 10^{-3}$	$8.87 \times 10^{-2} \pm 6.43 \times 10^{-3}$
k_{cat}/K_m (μM^{-1}· min^{-1})	$2.51 \times 10^{-3} \pm 4.37 \times 10^{-4}$	$4.91 \times 10^{-3} \pm 2.63 \times 10^{-4}$

The plus/minus represents the standard deviation of technical replicates ($n = 3$).

2.56 μM, k_{cat} of $2.71 \times 10^{-2} \pm 2.13 \times 10^{-3}$ min^{-1} and enzymatic efficiency (k_{cat}/K_m) of $2.49 \times 10^{-3} \pm 4.33 \times 10^{-4}$ μM^{-1}· min^{-1} against (±)-yateins-d_6 (**Supplementary Fig. S3** and **Table 2**).

To examine the selectivity of substrate enantiomers, (+)-yatein-d_6 and (−)-yatein-d_6 were individually subjected to enzyme assays with purified recAsDPS. GC-MS analysis of the assay products showed that deoxypodophyllotoxin-d_6 was produced only from (−)-yatein-d_6, whereas the (+)-enantiomer was not consumed and did not give the product (**Supplementary Figs. S4B c, S5**, and **Table 1**). This is in sharp contrast to the reactivity of PhDPS that accepts both (−)- and (+)-enantiomers of yatein (Tang et al. 2022). Kinetic analysis of recAsDPS with (−)-yatein-d_6 revealed the following values: V_{max} of 3.00 ± 0.05 nmol· min^{-1}· mg^{-1} protein, K_m of 22.57 ± 0.88 μM, k_{cat} of $0.11 \pm 1.76 \times 10^{-3}$ min^{-1} and k_{cat}/K_m of $5.01 \times 10^{-3} \pm 1.15 \times 10^{-4}$ μM^{-1}· min^{-1} (**Supplementary Fig. S3** and **Table 2**).

Structural comparison of AsDPS with PhDPS

Recently, protein structures of PhDPS in the presence of co-factor [Protein Data Bank (PDB) code, 7E37; DPS·Fe·2OG] or substrate (PDB code, 7E38; DPS· succinate· yatein) were solved and a catalytic mechanism for PhDPS-mediated cyclization of yatein to afford deoxypodophyllotoxin was proposed (Tang et al. 2022). By comparing the PhDPS structure with the predicted AsDPS structure, we attempted to elucidate the mechanism that induced the difference in selectivity of substrate enantiomers between these DPSs. Protein modeling of AsDPS was performed using AlphaFold2 (Jumper et al. 2021) and the predicted structure was then superimposed onto the coordinates of PhDPS structure (Tang et al. 2022). PyMOL was used to determine the root mean square deviation (RMSD) of each of the Cα atoms of the 313 amino acid residues of the AsDPS model from the corresponding Cα atom of the PhDPS structure (7E38) to evaluate the similarity of the overall 3D structure of the AsDPS model to the PhDPS structure. The RMSD value was 1.67 Å for the 313 Cα atoms, which was <2.0 Å. This indicates that their 3D structures were relatively similar (Gan et al. 2002). Additionally, in the superimposition, the positions of the iron-binding triad HXDXnH motif (His200, Asp202, and His257 in AsDPS) and the 2OG-binding triad YXnRXS motif (Tyr185, Arg268, and Ser270 in AsDPS), the highly conserved motifs among plant 2-ODDs, in the AsDPS model were found to be close to those in the PhDPS structure (**Fig. 5A**) (Hegg and Que 1997, Jin et al. 2020, Takehara et al. 2020, Tang et al. 2022). Taken together, we postulated that the substrate-binding position in AsDPS was almost the same as that in PhDPS.

The superimposition also showed that, within the pockets of substrate and co-factors of AsDPS and PhDPS, 15 amino acid residues were close to the lignan substrates, (−)-yatein and (+)-yatein (**Fig. 5B, C, D**). Among them, we detected that nine amino acid residues differ between the two DPSs, namely, Leu95, Val99, Tyr108, Arg181, Thr183, Tyr305, Phe308, Gly309 and His315 of AsDPS, which correspond to Pro80, Thr86, Asn92, His165, Met167, Leu286, Cys289, Phe290 and Ala295 of PhDPS, respectively (**Fig. 5B, C**). Meanwhile, the others are conserved, namely, Leu179, Leu197, Lys203, Val259, Phe274 and Phe276 of AsDPS, corresponding to Leu163, Leu181, Lys187, Val241, Phe255 and Phe257 of PhDPS (**Fig. 5D**). Among these nine unconserved amino acid residues, Val99, Tyr108, Arg181 and Thr183 of AsDPS are located near the A and B aromatic rings of (−)- and (+)-yateins (**Fig. 5B**), whereas Leu95, Tyr305, Phe308, Gly309 and His315 are close to the D and E rings of (−)- and (+)-yateins (**Fig. 5C**). In addition, only Tyr305 of AsDPS and Leu286 of PhDPS are located close to the chiral carbon atoms C8 and C8′ of (−)- and (+)-yateins (**Fig. 5C**).

We next examined the possible contribution of Tyr305 in AsDPS to enantiomer recognition. We generated recAsDPS_Y305L mutant by site-directed mutagenesis. After confirming purification by sodium dodecyl sulfate–polyacrylamide gel electrophoresis (SDS-PAGE) (**Supplementary Fig. S1**), purified recAsDPS_Y305L was subjected to enzyme assay with (±)-yateins-d_6, (−)-yatein-d_6 and (+)-yatein-d_6 as substrates. Unexpectedly, however, GC-MS analysis of the reaction products detected no formation of deoxypodophyllotoxin from any of the yatein substrates (**Supplementary Fig. S5** and **Table 1**). Blue-Native PAGE (BN-PAGE) and differential scanning fluorimetry (DSF) assays (**Supplementary Figs. S6, S7**) (Wittig et al. 2006, Phillips and de la Peña 2011,

Downloaded from https://academic.oup.com/pcp/article/64/12/1436/7329445 by guest on 22 May 2025

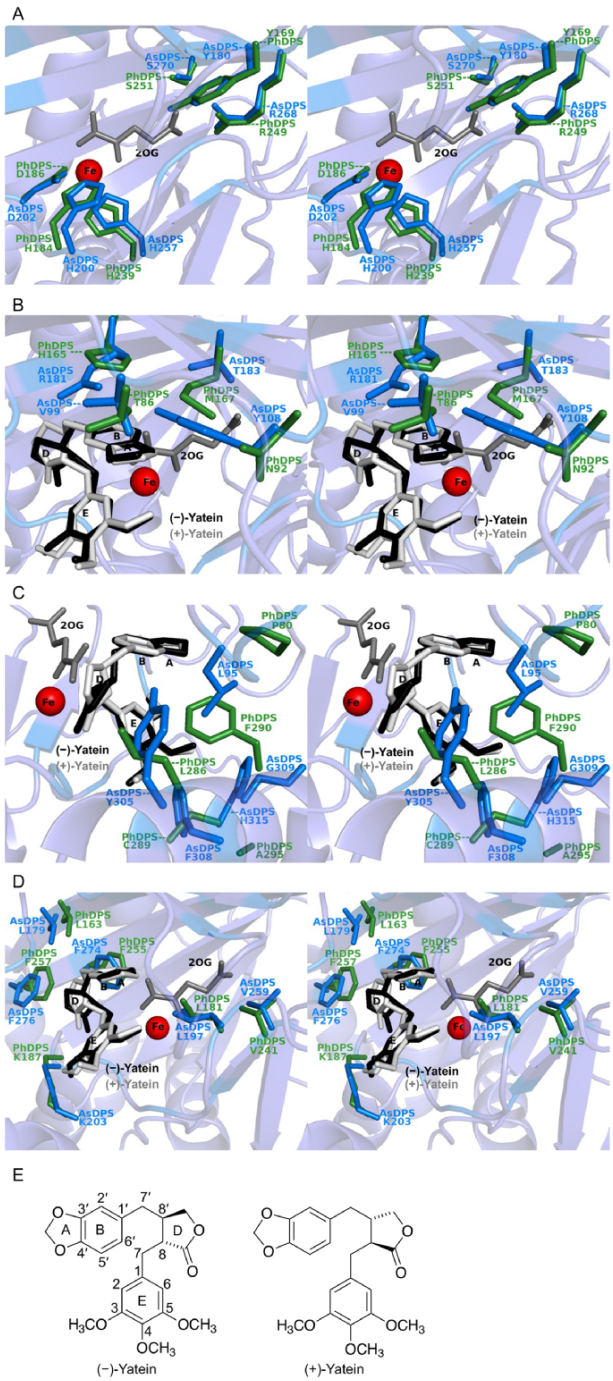


Fig. 5 Stereograms showing the superimposition of the protein model of AsDPS onto the protein structure of PhDPS. Blue: AsDPS, green: PhDPS, red sphere: Fe, dark gray: 2OG, black: (−)-yatein, gray: (+)-yatein. A: The iron-binding triad HXDXnH motif (His200, Asp202 and His257 in AsDPS; His184, Asp186 and His239 in PhDPS) and the 2OG-binding triad YXnRXS motif (Tyr185, Arg268 and Ser270 in AsDPS; Tyr169, Arg249 and Ser251 in PhDPS). B: Four amino acid residues (Val99, Tyr108, Arg181 and Thr183 in AsDPS; Thr86, Asn92, His165 and Met167 in PhDPS) that are not conserved between AsDPS and PhDPS are located near the A and B rings of yatein in the substrate pockets. C: Five unconserved amino acid residues (Leu95, Tyr305, Phe308, Gly309 and His315 in AsDPS; Pro80, Leu286, Cys289, Phe290 and Ala295 in PhDPS) between AsDPS and PhDPS are close to the D and E rings of yatein in the substrate pockets. D: Six conserved amino acid residues (Leu179, Leu197, Lys203, Val259, Phe274 and Phe276 in AsDPS; Leu163, Leu181, Lys187, Val241, Phe255 and Phe257 in PhDPS) are in the substrate pockets. E: Structures of (−)- and (+)-yateins.

Biter et al. 2016) did not show any significant differences in the protein mobility and melt curves between the mutants and the wild type (WT), indicating that there were no significant differences in the whole 3D structures between recAsDPS_Y305L and recAsDPS_WT.

Next, to evaluate the interaction between substrates and the aromatic ring and phenolic hydroxy group of Tyr305 of AsDPS_WT, recAsDPS_Y305F and recAsDPS_Y305A mutants were prepared as mentioned earlier. After purification (**Supplementary Fig. S1**), recAsDPS_Y305F and recAsDPS_Y305A were subjected to the assay with (±)-yateins-d_6, (−)-yatein-d_6 and (+)-yatein-d_6 as substrates. GC-MS analysis showed that recAsDPS_Y305F mutant exhibited almost the same activity as the WT. The mutant catalyzed the cyclization of (−)-yatein-d_6 to deoxypodophyllotoxin-d_6 (**Supplementary Fig. S5** and **Table 1**), whereas the (+)-enantiomer was not consumed and not converted into deoxypodophyllotoxin (**Supplementary Fig. S5** and **Table 1**). By contrast, recAsDPS_Y305A was not active for any of the yatein substrates (**Supplementary Fig. S5** and **Table 1**).

Kinetic analysis showed that the K_m values of recAsDPS_Y305F were 19.17 ± 4.8 and 18.12 ± 1.72 μM, the V_{max} values were 1.22 ± 0.13 and 2.35 ± 0.17 nmol· min^{-1}· mg^{-1} protein, the k_{cat} values were $4.61 \times 10^{-2} \pm 5.00 \times 10^{-3}$ and $8.87 \times 10^{-2} \pm 6.43 \times 10^{-3}$ min^{-1} and the k_{cat}/K_m values were $2.51 \times 10^{-3} \pm 4.37 \times 10^{-4}$ and $4.91 \times 10^{-3} \pm 2.63 \times 10^{-4}$ μM^{-1}· min^{-1} against (±)-yateins-d_6 and (−)-yatein-d_6, respectively (**Supplementary Fig. S3** and **Table 2**). These results indicated that the enzymatic efficiency of recAsDPS_Y305F was not significantly reduced compared with that of the WT enzyme (**Supplementary Fig. S3** and **Table 2**).

Discussion

A 2-ODD from *P. hexandrum* was found to catalyze the cyclization of yatein to give deoxypodophyllotoxin (Lau and Sattely 2015) and named DPS (Tang et al. 2022). This suggested that *A. sylvestris* also possesses 2-ODD-type DPS. However, given that the biosynthesis of yatein, deoxypodophyllotoxin and podophyllotoxin evolved independently in *Podophyllum* and *Anthriscus* (Yamamura et al. 2023), *Anthriscus* DPS might belong to another type of enzyme such as CYP, as in flavone synthesis, which can be catalyzed both by 2-ODDs (FNS I) (Kawai et al. 2014) and by CYPs (FNS II) (Lam et al. 2021). In the present study, we first analyzed the correlation of RNA-seq FPKM data between *Anthriscus* putative sequences encoding 2-ODD and CYP and a gene encoding AsSNYOMT that catalyzes 4,5-*O*,*O*-dimethylthujaplicatin formation. Next, based on biochemical characterization of the corresponding recombinant protiens,

Downloaded from https://academic.oup.com/pcp/article/64/12/1436/7329445 by guest on 22 May 2025

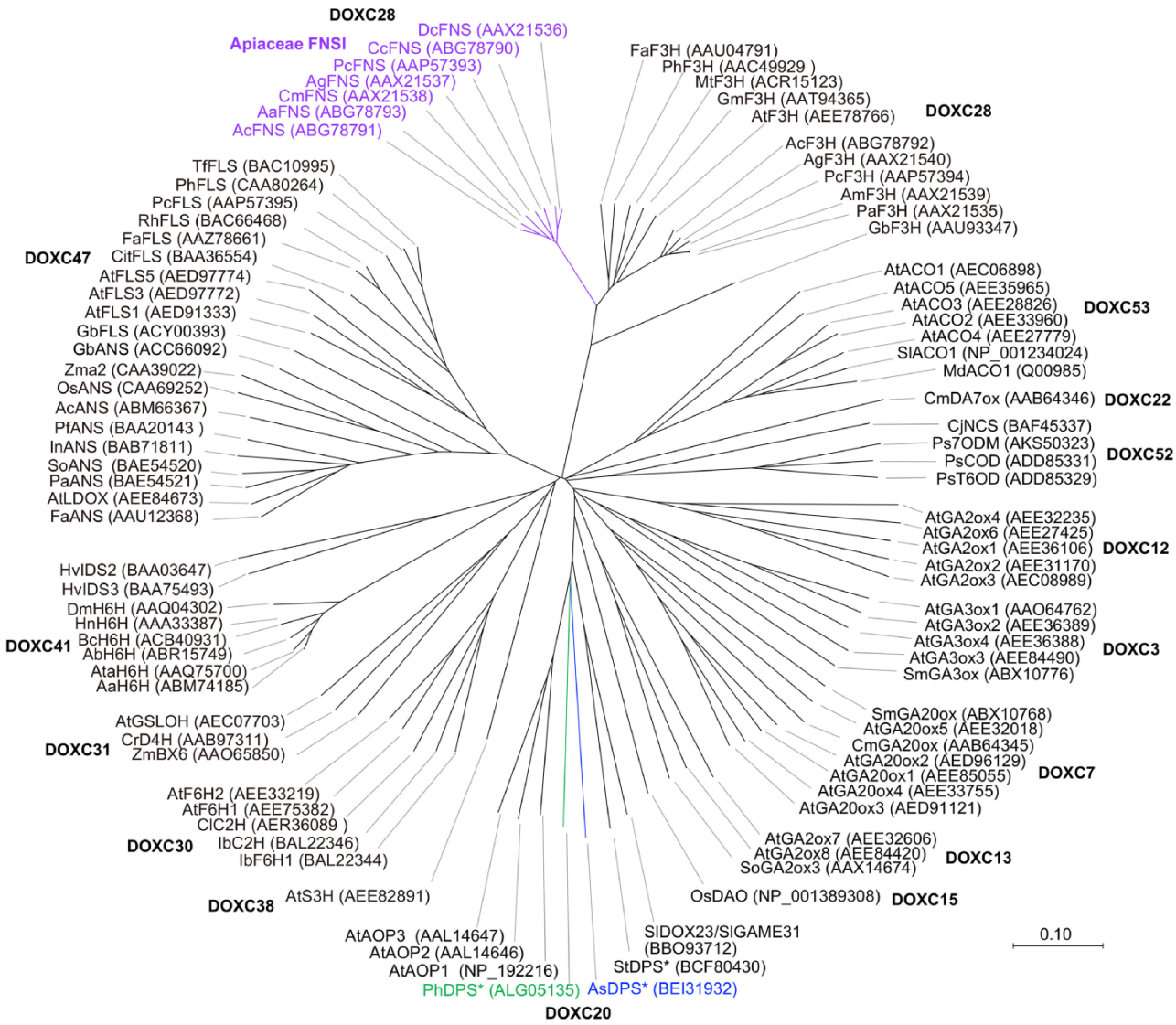


Fig. 6 The phylogenetic tree of AsDPS and other plant 2-ODDs (Kawai et al. 2014, Lau and Sattely 2015, Cárdenas et al. 2019, Nakayasu et al. 2020, Akiyama et al. 2021). DDBJ/EMBL/GenBank/NCBI accession numbers in parentheses are provided beside each name. *PhDPS *P. hexandrum* deoxypodophyllotoxin synthase (Tang et al. 2022), AsDPS: *A. sylvestris* deoxypodophyllotoxin synthase (this study), StDPS: *Solanum tuberosum* dioxygenase for potato solanidane synthesis (Akiyama et al. 2021).

we identified an As2-ODD enzyme that catalyzes the cyclization of yatein to afford deoxypodophyllotoxin, which was referred to as AsDPS. Therefore, CYP screening was not continued.

Given that *AsDPS* and *AsSNYOMT* exhibited high co-expression efficiency together with a gene encoding AsTJOMT that is another enzyme in the (deoxy)podophyllotoxin biosynthetic pathway (**Figs. 1**, **2** and **Supplementary Fig. S8**) (Ragamustari et al. 2013, Yamamura et al. 2023), the co-expression analysis may be useful to identify unknown enzyme genes that are involved in the (deoxy)podophyllotoxin biosynthesis in *A. sylvestris*. In addition, the analysis would also help to examine the presence of common transcription factors that coordinately orchestrate the (deoxy)podophyllotoxin biosynthesis.

Among three subclasses of plant 2-ODDs, DOXA, DOXB and DOXC (Kawai et al. 2014), both AsDPS and PhDPS belong to DOXC. The 2-ODDs of the DOXA and DOXB classes are involved in the oxidative demethylation of alkylated nucleic acids and histones and proline 4-hydroxylation in cell wall protein synthesis, respectively (Kawai et al. 2014). On the other hand, plant 2-ODDs belonging to the DOXC-class are involved in various reactions of secondary metabolism such as hydroxylation, demethylation, cyclization and halogenation (Hagel and Facchini 2010, Kawai et al. 2014, Farrow and Facchini 2015, Lau and Sattely 2015, Martinez and Hausinger 2015, Kim et al. 2020). Among the DOXC-class 2-ODDs, the FNS I enzymes that are specifically produced by Apiaceae plants belong to the DOXC28 clade (**Fig. 6**) (Kawai et al. 2014). However, although

Downloaded from https://academic.oup.com/pcp/article/64/12/1436/7329445 by guest on 22 May 2025

A. sylvestris belongs to Apiaceae, phylogenetic analysis revealed that AsDPS does not reside in the DOXC28 clade, but it is included in the DOXC20 clade together with PhDPS (**Fig. 6**). In addition, this clade harbors 2-ODD enzymes with various functions, e.g. α-tomatine 23-hydroxylase (Sl23DOX/SlGAME31) (Cárdenas et al. 2019, Nakayasu et al. 2020), dioxygenase for potato solanidane synthesis (Akiyama et al. 2021) and *Arabidopsis thaliana* (At) AOP2 and AtAOP3 (Kliebenstein et al. 2001) involved in steroidal glycoalkaloid biosynthesis and glucosinolate biosynthesis, respectively (**Fig. 6**) (Kawai et al. 2014).

While AsDPS and PhDPS exhibit moderate amino acid sequence identity (40.8%), AsDPS and PhDPS showed completely different selectivity for substrate enantiomers. PhDPS converts both (−)- and (+)-yateins into the products (Tang et al. 2022), whereas AsDPS cyclizes only (−)-yatein to afford the product (**Supplementary Figs. S4B, S5** and **Table 1**). Therefore, AsDPS and PhDPS have probably been acquired in each species by parallel evolution (Weng 2014) in the 2-ODD superfamily.

To examine the amino acid residues that are involved in the substrate enantiomer recognition, we prepared a protein model of AsDPS using the AlphaFold2 program (Jumper et al. 2021). Then, the model was superimposed onto PhDPS structure (Tang et al. 2022). Based on the comparison, we postulated that the substrate binding position in AsDPS was almost the same as that in PhDPS. In the pockets of substrate and co-factors of the AsDPS model, there was no severe crash (C–C contact of <3.3 Å) between AsDPS protein residues and the placed 2OG, (−)-yatein and (+)-yatein. Fifteen amino acid residues were found to be close to the lignan substrate, (−)- and (+)-yateins (**Fig. 5B, C, D**). Among them, nine amino acid residues differed between the two DPSs: Leu95, Val99, Tyr108, Arg181, Thr183, Tyr305, Phe308, Gly309 and His315 of AsDPS, which correspond to Pro80, Thr86, Asn92, His165, Met167, Leu286, Cys289, Phe290 and Ala295 of PhDPS, respectively (**Fig. 5B, C**). In particular, only Tyr305 of AsDPS and Leu286 of PhDPS are located close to the chiral carbon atoms C8 and C8′ of (−)- and (+)-yateins (**Fig. 5C**).

These results prompted us to examine the possible role of Tyr305 of AsDPS in substrate enantiomer recognition, which corresponds to Leu286 of PhDPS, by comparing the substrate enantiomer selectivity of recAsDPS_Y305L mutant with that of the WT. Unexpectedly, however, the mutation resulted in the complete loss of cyclization activity (**Supplementary Fig. S5** and **Table 1**). In addition, the substitution of Tyr305 with a smaller and non-aromatic residue, Ala, also resulted in the complete loss of cyclization activity (**Supplementary Fig. S5** and **Table 1**). Because there was no significant change in the whole 3D structures of recAsDPS_Y305L and recAsDPS_Y305A from recAsDPS_WT as confirmed by BN-PAGE and DSF assays (**Supplementary Figs. S6, S7**) (Wittig et al. 2006, Phillips and de la Peña 2011, Biter et al. 2016), these results strongly suggest that the loss of enzyme activity was not due to disruption of the whole protein structures but rather due to the loss of

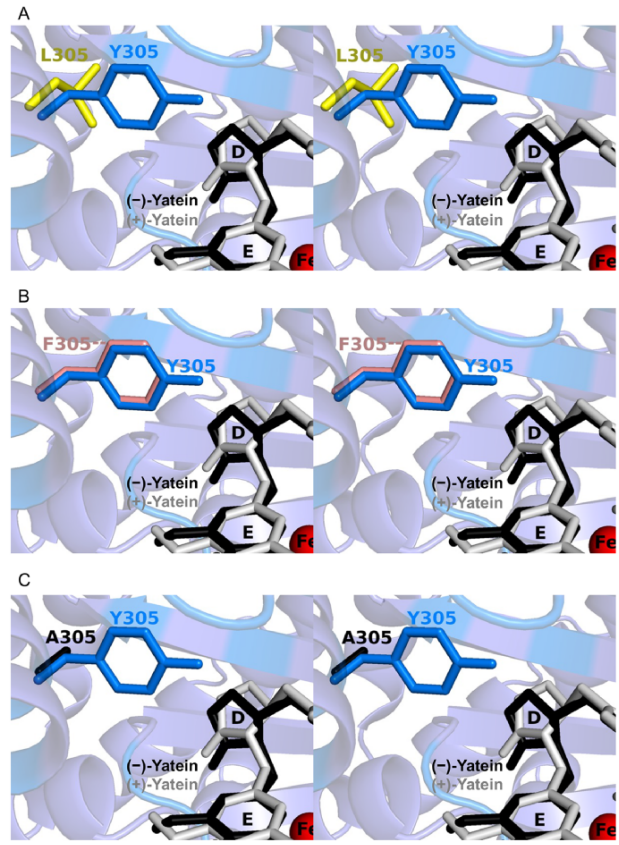


Fig. 7 Stereograms showing the positions of the mutated amino acid residues in the substrate pocket of AsDPS_WT and AsDPS mutants (AsDPS_Y305L, AsDPS_Y305F and AsDPS_Y305A). (A) AsDPS_Y305L and AsDPS_WT, (B) AsDPS_Y305F and AsDPS_WT, (C) AsDPS_Y305A and AsDPS_WT. Blue: Y305 of AsDPS_WT, yellow: L305 of AsDPS_Y305L, pink: F305 of AsDPS_Y305F, black: A305 of AsDPS_Y305A, red sphere: Fe, black: (−)-yatein and gray: (+)-yatein.

interaction of these amino acid residues (Leu and Ala) with (−)-yatein (**Fig. 7A, C**). In contrast, recAsDPS_Y305F still possessed the same substrate enantiomer selectivity and almost the same kinetic properties as recAsDPS_WT (**Supplementary Figs. S3, S5**, and **Tables 1** and **2**). This showed that the phenolic hydroxy group of Tyr305 of AsDPS is not essential to the cyclization reaction (**Fig. 7B**, **Supplementary Figs. S3, S5**, and **Tables 1** and **2**). It is strongly suggested that the amino acid side chain at the 305 position of AsDPS plays a critical role in the substrate recognition of yatein. However, the detailed interaction between these amino acid side chains at 305 position and substrates will need to be clarified by crystal structure analysis.

The optimal concentrations of 2OG and ascorbic acid for recAsDPS are lower by one to two orders of magnitude than those reported for PhDPS (Lau and Sattely 2015, Tang et al. 2022), indicating that AsDPS is inhibited by the high concentrations of 2OG and ascorbic acid. The inhibition of AsDPS by 2OG at a high concentration (**Fig. 4**) can plausibly be accounted for

Downloaded from https://academic.oup.com/pcp/article/64/12/1436/7329445 by guest on 22 May 2025

by the possibility that recAsDPS has another 2OG-binding site around the substrate-binding site.

Recently, Chang et al. (2019) clearly demonstrated that podorhizol was unlikely to be the intermediate in the PhDPS-mediated cyclization of yatein to deoxypodophyllotoxin, as the compound is an off-pathway product, even though podorhizol is formed in the assay (Tang et al. 2022). Instead, they proposed the involvement of a benzyl radical and a benzyl cation as intermediates but not quinonemethide-like cation (Chang et al. 2019, Tang et al. 2022). However, the benzyl cation and quinonemethide-like cation are not independent molecular species but resonance contributors (or canonical structures) of a single resonance hybrid structure (the square bracket in pathway II in **Supplementary Fig. S9**). A slightly modified mechanism is shown in pathway II of **Supplementary Fig. S9**, which includes the resonance hybrid structure including the benzyl cation structure (**Supplementary Fig. S9**, a in pathway II) and the quinonemethide-like cation structure (**Supplementary Fig. S9**, d in pathway II).

In conclusion, we identified and characterized AsDPS. AsDPS and PhDPS shared moderate amino acid sequence identity, whereas both DPSs showed marked differences in terms of substrate enantiomer selectivity. Protein modeling using AlphaFold2 and site-directed mutagenesis indicated that the Tyr305 residue of AsDPS, in particular its aromatic ring, probably contributes to substrate recognition. This study provides a better understanding of podophyllotoxin biosynthesis in *A. sylvestris* and of 2-ODD superfamily enzymes widely involved in various metabolisms in plants.

Materials and Methods

Chemicals

(±)-Yateins were previously synthesized and (−)-deoxypodophyllotoxin was previously isolated (Sakakibara et al. 2003). (±)-[4,5-(OC^2H_3)$_2$]Yateins [(±)-yateins-d_6] were prepared by dideutromethylation of (±)-5-hydroxypluviatolides that were prepared previously (Sakakibara et al. 2003). (±)-[4,5-(OC^2H_3)$_2$]Yateins: δ_H ($CDCl_3$) 6.70 (1H, d, *J* 8.0), 6.47 (1H, d, *J* 8.4), 6.46 (1H, s), 6.35 (2H, s), 5.91–5.96 (2H, m), 4.18 (1H, dd, *J* 8.6 and 7.0), 3.88 (1H, dd, *J* 8.8 and 7.6), 3.83 (3H, s), 2.93 (1H, dd, *J* 13.6 and 5.2), 2.88 (1H, dd, *J* 13.6 and 6.4), 2.44–2.66 (4H, m); electron impact mass spectrum *m/z* 406 (M^++6, 64.1%), 405 (2.6), 404 (0), 403 (0), 402 (0), 187 (100), 135 (50.7). All other reagents were obtained from Nacalai Tesque, Inc. (Kyoto, Japan) or FUJIFLIM Wako Pure Chemicals Co., Ltd. (Osaka, Japan) unless otherwise noted.

Instrumentation

GC-MS was performed using the QP-2010 Plus GC-MS system and QP-2010 Ultra GC-MS system (Shimadzu Co., Kyoto, Japan). The GC-MS conditions were as follows: CBP10 column (Shimadzu Co.), 0.25 μm, 5.0 m × 0.22 mm; electron impact mode, 70 eV; injection temperature, 250°C; interface temperature, 250°C; ion source temperature, 250°C and column temperature, 160°C at $t = 0$ min, which was then raised to 250°C at 20°C min^{-1}. The MS analysis was conducted in scan mode at *m/z* range 50–700 and SIM mode for the confirmation of enzyme activity and the measurement for specific activity of recAs2-ODD-1, recAs2-ODD-2 (recAsDPS) and three recAsDPS mutants. For kinetic analysis of recAs2-ODD-2 (recAsDPS) and recAs2-ODD-2 mutant (recAsDPS_Y305F), SIM mode was used.

Chiral separation of (±)-yateins-d_6 and isolation of (+)- and (−)-yateins-d_6 were performed using a chiral high-performance liquid chromatography (HPLC) system composed of a CMB-20A series system controller, two LC-20AD series pumps, a SIL-20AC series automatic sampler, a CTO-20A series column oven set at 40°C and an SPD-20A series Prominence UV–VIS Detector at 254 nm (Shimadzu Co.). The column used was a Chiralpak IB-3 (2 mm × 250 mm, 3 μm; Daicel Corp., Osaka, Japan) eluted by ethanol/0.2% acetic acid in *n*-hexane (5/95 by vol.) at a flow rate of 0.3 ml· min^{-1} (Ragamustari et al. 2014). The optical rotation for yatein enantiomers was determined using the chiral HPLC system as described earlier and a JASCO OR-990 Chiral Detector (JASCO Corp., Ltd., Tokyo, Japan).

^{1}H NMR spectra were taken with a JEOL ECS-400 (400 MHz, JEOL Co., Akishima, Tokyo, Japan). Chemical shifts and coupling constants (*J*) were given in δ and Hz, respectively.

Concentrations of recombinant proteins were determined by the Bradford method (Bradford 1976) using a UV-2600 UV-VIS Spectrophotometer (Shimadzu Co.).

DSF assay was carried out in the CFX96 Touch Real-Time PCR Detection System (BIO-RAD Laboratories, Hercules, CA, USA). The temperature of the measurement program was raised from 4°C to 95°C, at intervals of 0.5°C with an equilibration time of 10 s at each temperature.

Total RNA samples and cDNA template preparation

Total RNA that was extracted from *A. sylvestris* previously (Yamamura et al. 2023) was used for preparing cDNAs using SuperScript III First-Strand Synthesis System for RT-PCR (Thermo Fisher Scientific, Rockford, IL, USA). The cDNAs were used as templates for the amplification of candidate genes by PCR.

tBLASTx analysis and correlation analysis

RNA-seq data (367,585 contigs) from *A. sylvestris* (Yamamura et al. 2023) were subjected to tBLASTx analysis using *PhDPS* (KT390173) sequence (Lau and Sattely 2015) as a query. Nine putative *2-ODD* contigs that shared high homology with the query were selected. After confirming the existence of CDS, the values of FPKM were calculated by Bowtie Mapping for putative *2-ODD* sequences. Then, the correlations of gene expression patterns between *AsSNYOMT* and *As2-ODD* candidate contigs were calculated using Microsoft Excel, and the contigs exhibiting co-expression efficiency of >0.8 were selected.

Plasmid construction of candidate genes and *E. coli* transformation

Each CDS of the candidate contigs was amplified from the cDNAs of *A. sylvestris* by PCR using the primer sets listed in **Supplementary Table S1**. After amplification, the PCR products were ligated into pCR4-TOPO using TOPO TA Cloning Kit (Thermo Fisher Scientific), in accordance with the manufacturer's protocol. Each construct was then transformed into *E. coli* TOP10 or DH5α competent cells. The constructs were extracted with QIAprep Spin Miniprep Kit (Qiagen, Hilden, Germany), in accordance with the manufacturer's protocol. After sequencing to confirm the accuracy of each construct, an *Nde*I site at the 5′-end and an *Xho*I or a *Not*I site at the 3′-end of the CDS of *As2-ODD-1* were introduced by PCR using the gene-specific primers (**Supplementary Table S2**). The PCR product was ligated into pCR4-TOPO and then transformed into *E. coli* TOP10 or DH5α competent cells as mentioned earlier. After extraction of the construct using QIAprep Spin Miniprep Kit (Qiagen), the plasmid pCR4-TOPO-As2-ODD-1 was digested with *Nde*I and *Not*I or *Xho*I (New England Biolabs Inc., Beverly, MA, USA) and then ligated into pCold TF DNA (Takara Bio, Otsu, Japan), pCold1 (Takara Bio), pCold2 (Takara Bio), pET-15b (Merck KGaA, Darmstadt, Germany), pET-23a (Merck KGaA) and pET-30a (Merck KGaA) vectors with a T4 ligase kit (New England Biolabs), in accordance with the manufacturer's protocol. Then, the constructs were transformed into *E. coli* DH5α competent cells to be amplified. The constructs were extracted with QIAprep Spin Miniprep Kit (Qiagen), in accordance with the manufacturer's protocol. After sequence confirmation, the construct was transformed into *E. coli* BL21 (DE3) competent cells. For *As2-ODD-2* (*AsDPS*), an *Nde* I site at the 5′-end and a *Not* I site at the 3′-end of the CDS of *As2-ODD-2* (*AsDPS*) were introduced

Downloaded from https://academic.oup.com/pcp/article/64/12/1436/7329445 by guest on 22 May 2025

with gene-specific primers (**Supplementary Table S2**) and then ligated into pET-30a (Merck KGaA) vector with a T4 ligase kit as mentioned earlier. Then, the constructs were transformed into *E. coli* DH5α competent cells to be amplified. The constructs were extracted with QIAprep Spin Miniprep Kit (Qiagen), in accordance with the manufacturer's protocol. After sequence confirmation, the construct was transformed into *E. coli* BL21 (DE3) competent cells. These were used to express the recombinant proteins of As2-ODD candidates.

Expression and purification of recAs2-ODDs

Each bacterium harboring the plasmid pCold TF DNA-As2-ODD-1 and pET-30a-As2-ODD-2 (AsDPS) was cultured at 37°C in 100 ml of LB medium containing 100 mg· l^{-1} ampicillin and 50 mg· l^{-1} kanamycin, respectively. Upon the culture reaching A_{600} of 0.6, isopropyl-β-D-thiogalactopyranoside was added to the culture at a final concentration of 0.4 mM to induce protein expression of recAs2-ODD-1 and recAs2-ODD-2 (recAsDPS), and the culture was incubated for 24 h at 15°C and for 6 h at 28°C, respectively. After harvesting the cells by centrifugation (2,000×*g*, 4°C, 20 min), the cell pellet was stored at −80°C until use.

To prepare crude enzymes of recAs2-ODD-1 and rec2-ODD-2 (recAsDPS), the *E. coli* pellets were resuspended in lysis buffer [20 mM Tris, 5 mM imidazole, 500 mM NaCl, 10% (vol/vol) glycerol, 14 mM β-mercaptoethanol, pH7.5] and then lysed by sonication using a Misonix S-4000 sonicator (QSonica, LLC, Newtown, CT, USA). After centrifugation of the lysate (14,000×*g*, 4°C, 10 min), the supernatant was subjected to the enzyme assay as the crude enzyme.

For recAs2-ODD-2 (recAsDPS) purification, the crude enzyme was subjected to affinity chromatography using a His-bind resin (Merck KGaA). Next, the column was washed with lysis buffer, wash buffer 60 [20 mM Tris, 60 mM imidazole, 500 mM NaCl, 10% (vol/vol) glycerol, 14 mM β-mercaptoethanol, pH7.5] and wash buffer 80 [20 mM Tris, 80 mM imidazole, 500 mM NaCl, 10% (vol/vol) glycerol, 14 mM β-mercaptoethanol, pH7.5]. After washing, the recombinant protein was eluted from the His-bind resin using an elution buffer [20 mM Tris, 250 mM imidazole, 500 mM NaCl, 10% (vol/vol) glycerol, 14 mM β-mercaptoethanol, pH7.5]. The eluted protein was then desalted in 50 mM Tris-HCl buffer [10% (vol/vol) glycerol, 14 mM β-mercaptoethanol, pH7.0] by Sephadex® G-25 Coarse (Sigma-Aldrich Co. LLC, St. Louis, MO, USA). Finally, the purity of the recombinant protein was checked by SDS-PAGE.

Enzyme activity for yatein cyclization

Yatein cyclization assays with recAs2-ODD-1 and recAs2-ODD-2 were performed with the following two reaction conditions. One was composed of 20 μg of crude enzyme, 10 mM 2OG, 10 mM ascorbic acid, 0.5 mM $FeSO_4$ and 20 μM (±)-yateins in 50 mM Tris-HCl buffer (pH7.5) (total volume, 100 μl), which is in accordance with the work by Lau and Sattely (2015). The other (total volume, 100 μl) contained 20 μg of crude enzymes, 0.1 mM 2OG, 0.1 mM ascorbic acid, 50 μM $FeSO_4$ and 10 μM (±)-yateins in 50 mM Tris-HCl buffer (pH7.5). Assays using heat-denatured enzymes served as negative controls. After incubation at 30°C for 1 h, the reaction was terminated by adding 500 μl of ethyl acetate, and reaction products and residual substrate were extracted with ethyl acetate. The extraction was repeated once, and the combined ethyl acetate solutions were washed with a saturated NaCl solution (100 μl), dried over anhydrous Na_2SO_4 and dried under a high vacuum. The reaction products obtained were dissolved in *N,O*-bis(trimethylsilyl)acetamide (8 μl). After heating at 60°C for 45 min, an aliquot (0.8 μl) of the solution was analyzed by GC-MS using a Shimadzu QP-2010 Plus GC-MS system.

The assay with recAs2-ODD-1 was repeated with enzyme reaction solution (100 μl) containing 20 μg of crude recAs2-ODD-1, 0.1 mM 2OG, 0.1 mM ascorbic acid, 50 μM $FeSO_4$ and 10 μM (±)-yateins-d_6 in 50 mM Tris-HCl buffer (pH7.5). After incubation at 30°C for 1 h, the reaction was terminated by adding 500 μl of ethyl acetate containing 0.15 nmol (−)-deoxypodophyllotoxin as an internal standard. The extraction without the internal standard was repeated once, and the combined ethyl acetate solutions were washed with a saturated NaCl solution (100 μl), dried over anhydrous Na_2SO_4 and dried under a high vacuum and subjected to GC-MS analysis as mentioned earlier.

To optimize 2OG and ascorbic acid concentrations, enzyme assays were conducted with the following conditions: for 2OG, 20 μg of purified recAsDPS (recAs2-ODD-2); 1 μM, 5 μM, 10 μM, 50 μM, 100 μM, 1 mM and 10 mM 2OG; 0.1 mM ascorbic acid; 50 μM $FeSO_4$ and 10 μM (±)-yateins-d_6 in 50 mM Tris-HCl buffer (pH7.0); for ascorbic acid, 20 μg of purified recAsDPS (recAs2-ODD-2); 50 μM 2OG; 1 μM, 10 μM, 50 μM, 100 μM, 500 μM, 1 mM and 10 mM ascorbic acid; 50 μM $FeSO_4$ and 10 μM (±)-yateins-d_6 in 50 mM Tris-HCl buffer (pH7.0). After incubation at 30°C for 1 h, the reaction was terminated by adding 500 μl of ethyl acetate containing 0.15 nmol (−)-deoxypodophyllotoxin as an internal standard. The extraction without the internal standard was repeated once, and the combined ethyl acetate solutions were washed with a saturated NaCl solution (100 μl), dried over anhydrous Na_2SO_4 and dried under a high vacuum and subjected to GC-MS analysis as mentioned earlier.

Specific activity was determined using a stable isotope dilution method by comparing the M^++6 intensity of the enzyme reaction product with M^+ of the authentic (−)-deoxypodophyllotoxin.

Optimal temperature and pH of recAsDPS (recAs2-ODD-2)

For optimal temperature determination, the enzyme reaction solution (total volume 100 μl) contained 20 μg of purified recAsDPS (recAs2-ODD-2), 50 μM 2OG, 500 μM ascorbic acid, 50 μM $FeSO_4$ and 10 μM (±)-yateins-d_6 in 50 mM Tris-HCl buffer (pH7.0). Enzyme reactions were carried out at 10°C, 20°C, 25°C, 30°C and 40°C for 1 h. For optimal pH determination, assays were performed using the same enzyme reaction components as for the optimal temperature determination but with the following buffer solutions: 50 mM Tris-HCl buffer (pH 7.0, 7.5, 8.0, 8.5 and 9.0), 50 mM potassium phosphate (KPB) buffer (pH 5.5, 6.0, 6.5, 7.0 and 7.5) and 50 mM sodium acetate buffer (pH 5.0 and 5.5). Enzyme reactions were carried out at 20°C for 1 h. After incubation for 1 h, the reactions were terminated by adding 500 μl of ethyl acetate containing 0.15 nmol (−)-deoxypodophyllotoxin as an internal standard. The ethyl acetate extracts were subjected to GC-MS analysis, and specific activity was determined as given earlier.

Reaction kinetics of recAsDPS (recAs2-ODD-2)

To measure kinetic constants, varying concentrations of (±)-yateins-d_6 (0, 1, 2, 5, 10, 30 and 50 μM) or (−)-yatein-d_6 (0, 1, 2, 5, 10, 30 and 50 μM) were incubated in the presence of 50 μM 2OG, 500 μM ascorbic acid, 50 μM $FeSO_4$ and 30 μg of purified recAsDPS (recAs2-ODD-2), in 50 mM Tris-HCl (pH 7.0) (total volume 100 μl). Kinetic constants were calculated based on Michaelis–Menten kinetics using Microsoft Excel and GraphPad Prism 8 (GraphPad Software, San Diego, CA, USA).

Protein structure modeling of AsDPS_WT and three AsDPS mutants

The protein structures of AsDPS_WT and three AsDPS mutants (AsDPS_Y305L, AsDPS_Y305F and AsDPS_Y305A) were predicted using AlphaFold2 (Jumper et al. 2021). To perform the superimposition of (+)- and (−)-yateins, and cofactors (2OG and Fe) with their protein models, two sets of protein structure information of PhDPS with Fe and 2OG (PDB, 7E37) and with Fe, succinate and (±)-yateins (PDB 7E38) were acquired from PDB (Tang et al. 2022). Then, succinate in the 7E38 structure was replaced with 2OG, to which the AsDPS models were superimposed. Each protein model was analyzed, and figures were generated using PyMOL Molecular Graphics System Version 2.5.2 (Schrödinger, Inc., New York, NY, USA).

Site-directed mutagenesis of AsDPS

AsDPS mutants (*AsDPS_Y305L*, *AsDPS_Y305F* and *AsDPS_Y305A*) were generated using PrimeSTAR® Mutagenesis Basal Kit (Takara Bio) with the plasmid pET-30a-AsDPS as the template and the primer sets (**Supplementary Table S3**). Expression and purification of recAsDPS mutants were conducted as given

Downloaded from https://academic.oup.com/pcp/article/64/12/1436/7329445 by guest on 22 May 2025

earlier. Enzyme assays were conducted using the enzyme reaction solution (total volume 100 μl) containing 30 μg of each purified recAsDPS mutant, 50 μM 2OG, 500 μM ascorbic acid, 50 μM $FeSO_4$ and 10 μM yatein [(±)-yateins-d_6, (−)-yatein-d_6, or (+)-yatein-d_6] in 50 mM Tris-HCl buffer (pH7.0). After incubation at 20°C for 10 min, the reaction was terminated by adding 500 μl of ethyl acetate containing 0.15 nmol (−)-deoxypodophyllotoxin as an internal standard. The ethyl acetate extracts were subjected to GC-MS analysis, and specific activity was determined as mentioned earlier. Kinetic analysis of recAsDPS_Y305F was performed in the same manner as above.

The conversion rate of (−)- and (+)-yatein in enzyme assays of recAsDPS and three recAsDPS mutants

Enzyme assays were conducted using the enzyme reaction solution (total volume 100 μl) containing 20 μg of purified recAsDPS_WT or recAsDPS mutants (AsDPS_Y305L, AsDPS_Y305F and AsDPS_Y305A), 50 μM 2OG, 500 μM ascorbic acid, 50 μM $FeSO_4$ and 2 μM yatein-d_6 [(−)-yatein-d_6 or (+)-yatein-d_6] in 50 mM Tris-HCl buffer (pH7.0). After incubation at 20°C for 10 min, the reaction was terminated by adding 500 μl of ethyl acetate containing 0.2 nmol (±)-yateins and 0.1 nmol (−)-deoxypodophyllotoxin as internal standards. The ethyl acetate extracts were subjected to GC-MS analysis as given earlier. Each conversion rate was calculated by comparison of the peak area of the residual amount of substrate in each assay with the peak area of (±)-yateins as an internal standard.

BN-PAGE of recAsDPS_WT and three recAsDPS mutants

BN-PAGE of the purified proteins of recAsDPS_WT and three recAsDPS mutants (AsDPS_Y305L, AsDPS_Y305F and AsDPS_Y305A) was performed using NativePAGE™ Sample Prep Kit (Thermo Fisher Scientific), NativePAGE™ Running Buffer Kit (Thermo Fisher Scientific), NativePAGE™ 4–16% Bis-Tris Gel (1.0 mm × 10 well) (Thermo Fisher Scientific) and Mini Gel Tank (Thermo Fisher Scientific) according to the NativePAGE™ Bis-Tris Gels Protocol (Protocol Pub. No. MAN0007893 Rev. 1.0) (Thermo Fisher Scientific).

DSF assay of recAsDPS_WT and two recAsDPS mutants (AsDPS_Y305L and AsDPS_Y305A)

DSF assays were carried out according to the protocol of Protein Thermal Shift Assays Made Easy with the Bio-Rad™ Family of CFX Real-Time PCR Detection Systems (BIO-RAD Laboratories). After the purification of recAsDPS_WT and two recAsDPS mutants (recAsDPS_Y305L and recAsDPS_Y305A), DSF assays were performed in three conditions in a 96-well plate with 20 μl of solution at the same time. As the first condition, the mixtures contained 15 μl of purified recombinant proteins (recAsDPS_WT: 20 μg, recAsDPS_Y305L: 32 μg, recAsDPS_Y305A: 15 μg), 2 μl of 50 × SYPRO Orange Protein Gel Stain (Thermo Fisher Scientific) and 3 μl of distilled water. To verify whether 2OG and substrates contribute to the stabilization of each enzyme, water of the first condition was changed to 3 μl of 100 μM (±)-yateins and 3 μl of 100 μM 2OG, respectively, as second and third conditions. Each experimental condition was conducted in triplicate. All data were analyzed using CFX Maestro software.

Phylogenetic analysis and alignment of amino acid sequences

The amino acid sequences of 2-ODDs were aligned using the MUSCLE program in MEGA11 software (Edgar 2004, Tamura et al. 2021). The phylogenetic tree was constructed using the neighbor-joining method (Saitou and Nei 1987) with MEGA11 (Tamura et al. 2021).

Supplementary Data

Supplementary data are available at *PCP* online.

Data Availability

All data necessary to evaluate the conclusions in this study are included in the published paper and its Supplementary data. Sequence data generated in this study can be accessed in the DNA Data Bank of Japan (DDBJ)/European Molecular Biology Laboratory Nucleotide Sequence Database (EMBL)/GenBank data libraries under the accession number (*AsDPS*, LC769120). RNA-seq data of *A. sylvestris* can be accessed in the National Center for Biotechnology Information (NCBI) Sequence Read Archive under accession numbers SRR16916378–SRR16916390. The DDBJ/EMBL/GenBank/NCBI accession numbers of proteins of the AsDPS and other 2-ODDs dealt in this study are provided in **Fig. 6** and as follows: AtGA3ox1 (AAO64762), AtGA3ox2 (AEE36389), AtGA3ox3 (AEE84490), AtGA3ox4 (AEE36388), SmGA3ox (ABX10776), AtGA20ox1 (AEE85055), AtGA20ox2 (AED96129), AtGA20ox3 (AED91121), AtGA20ox4 (AEE33755), AtGA20ox5 (AEE32018), CmGA20ox (AAB64345), SmGA20ox (ABX10768), AtGA2ox1 (AEE36106), AtGA2ox2 (AEE31170), AtGA2ox3 (AEC08989), AtGA2ox4 (AEE32235), AtGA2ox6 (AEE27425), AtGA2ox7 (AEE32606), AtGA2ox8 (AEE84420), SoGA2ox3 (AAX14674), OsDAO (NP_001389308), AtAOP1 (NP_192216), AtAOP2 (AAL14646), AtAOP3 (AAL14647), SlDOX23/GAME31 (BBO93712), StDPS (BCF80430), AsDPS (BEI31932), PhDPS (ALG05135), CmGA7ox (AAB64346), AcFNS (ABG78791), AcF3H (ABG78792), AmF3H (AAX21539), AgF3H (AAX21540), AaFNS (ABG78793), AgFNS (AAX21537), AtF3H (AEE78766), CmFNS (AAX21538), CcFNS (ABG78790), DcFNS (AAX21536), FaF3H (AAU04791), GbF3H (AAU93347), GmF3H (AAT94365), MtF3H (ACR15123), PcFNS (AAP57393), PcF3H (AAP57394), PhF3H (AAC49929), PaF3H (AAX21535), AtF6H2 (AEE33219), AtF6H1 (AEE75382), ClC2H (AER36089), IbF6H1 (BAL22344), IbC2H (BAL22346), AtGSLOH (AEC07703), CrD4H (AAB97311), ZmBX6 (AAO65850), AtS3H (AEE82891), AaH6H (ABM74185), AtaH6H (AAQ75700), AbH6H (ABR15749), BcH6H (ACB40931), DmH6H (AAQ04302), HvIDS2 (BAA03647), HvIDS3 (BAA75493), HnH6H (AAA33387), AcANS (ABM66367), AtAtFLS1 (AED91333), AtAtFLS3 (AED97772), AtAtFLS5 (AED97774), AtLDOX (AEE84673), CitFLS (BAA36554), FaFLS (AAZ78661), FaANS (AAU12368), GbFLS (ACY00393), GbANS (ACC66092), InANS (BAB71811), OsANS (CAA69252), PfANS (BAA20143), PcFLS (AAP57395), PhFLS (CAA80264), PaANS (BAE54521), RhFLS (BAC66468), SoANS (BAE54520), TfFLS (BAC10995), Zma2 (CAA39022), CjNCS (BAF45337), PsT6OD (ADD85329), PsP7ODM (AKS50323), PsCOD (ADD85331), AtACO4 (AEE27779), AtACO3 (AEE28826), AtACO2 (AEE33960), AtACO5 (AEE35965), AtACO1 (AEC06898), MdACO1 (Q00985) and SlACO1 (NP_001234024).

Downloaded from https://academic.oup.com/pcp/article/64/12/1436/7329445 by guest on 22 May 2025

Funding

Japan Society for the Promotion of Science (25292104, 18H02255 and 22H02406).

Acknowledgments

The authors express their sincere gratitude to the late Dr. Norikazu Sakakibara for his significant contribution to this study whereby he synthesised (±)-[4,5-(OC^2H_3)$_2$]yateins [(±)-yateins-d_6] when he was a graduate student in the laboratory of the corresponding author, Toshiaki Umezawa; this study contains the first published description of this compound. A part of this study was conducted using facilities in the Development and Assessment of Sustainable Humanosphere (DASH)/Forest Biomass Analytical System (FBAS) at Research Institute for Sustainable Humanosphere (RISH), Kyoto University, and the NMR spectrometer at the Joint Usage/Research Center (JURC)/Institute for Chemical Research (ICR), Kyoto University. The authors thank Mr. Fernando Satoshi Tutihashi for technical assistance. We also thank Prof. Yuki Tobimatsu and Mr. Koji Takaesu for their help with NMR measurements.

Author Contributions

M.Y., E.O. and T.U. designed the research. K.K., M.Y., B.M. N.S. and M.K. performed the research. K.K., M.Y., B.M., E.O. M.K., A.S., H.S. and T.U. analyzed the data. K.K., B.M., E.O. and T.U. wrote the article.

Disclosures

The authors have no conflicts of interest to declare.

References

Akimoto, K., Kitagawa, Y., Akamatsu, T., Hirose, N., Sugano, M., Shimizu, S., et al. (1993) Protective effects of sesamin against liver damage caused by alcohol or carbon tetrachloride in rodents. *Ann. Nutr. Metab.* 37: 218–224.

Akiyama, R., Watanabe, B., Nakayasu, M., Lee, H.J., Kato, J., Umemoto, N., et al. (2021) The biosynthetic pathway of potato solanidanes diverged from that of spirosolanes due to evolution of a dioxygenase. *Nat. Commun.* 12: 1–10.

Biswas, D., Biswas, P., Nandy, S., Mukherjee, A., Pandey, D.K. and Dey, A. (2020) Endophytes producing podophyllotoxin from *Podophyllum* sp. and other plants: a review on isolation, extraction and bottlenecks. *S. Afr. J. Bot.* 134: 303–313.

Biter, A.B., de La Peña, A.H., Thapar, R., Lin, J.Z. and Phillips, K.J. (2016) DSF guided refolding as a novel method of protein production. *Sci. Rep.* 6: 1–9.

Bradford, M.M. (1976) A rapid and sensitive method for the quantitation of microgram quantities of protein utilizing the principle of protein-dye binding. *Anal. Biochem.* 72: 248–254.

Canel, C., Moraes, R.M., Dayan, F.E. and Ferreira, D. (2000) Podophyllotoxin. *Phytochemistry* 54: 115–120.

Cárdenas, P.D., Sonawane, P.D., Heinig, U., Jozwiak, A., Panda, S., Abebie, B., et al. (2019) Pathways to defense metabolites and evading fruit bitterness in genus *Solanum* evolved through 2-oxoglutarate-dependent dioxygenases. *Nat. Commun.* 10: 1–13.

Chang, W.C., Yang, Z.J., Tu, Y.H. and Chien, T.C. (2019) Reaction mechanism of a nonheme iron enzyme catalyzed oxidative cyclization via C-C bond formation. *Org. Lett.* 21: 228–232.

Cravens, A., Payne, J. and Smolke, C.D. (2019) Synthetic biology strategies for microbial biosynthesis of plant natural products. *Nat. Commun.* 10: 1–12.

Edgar, R.C. (2004) MUSCLE: multiple sequence alignment with high accuracy and high throughput. *Nucleic Acids Res.* 32: 1792–1797.

Farrow, S.C. and Facchini, P.J. (2015) Papaverine 7-*O*-demethylase, a novel 2-oxoglutarate/Fe^{2+}-dependent dioxygenase from opium poppy. *FEBS Lett.* 589: 2701–2706.

Gan, H.H., Perlow, R.A., Roy, S., Ko, J., Wu, M., Huang, J., et al. (2002) Analysis of protein sequence/structure similarity relationships. *Biophys. J.* 83: 2781–2791.

Gao, Q., Yang, M. and Zuo, Z. (2018) Overview of the anti-inflammatory effects, pharmacokinetic properties and clinical efficacies of arctigenin and arctiin from *Arctium lappa L. Acta Pharmacol. Sin.* 39: 787–801.

Gordaliza, M., Garcia, P.A., Del Corral, J.M., Castro, M.A. and Gomez-Zurita, M.A. (2004) Podophyllotoxin: distribution, sources, applications and new cytotoxic derivatives. *Toxicon* 44: 441–459.

Guerram, M., Jiang, -Z.-Z. and Zhang, L.-Y. (2012) Podophyllotoxin, a medicinal agent of plant origin: past, present and future. *Chin. J. Nat. Med.* 10: 161–169.

Hagel, J.M. and Facchini, P.J. (2010) Dioxygenases catalyze the *O*-demethylation steps of morphine biosynthesis in opium poppy. *Nat. Chem. Biol.* 6: 273–275.

Hande, K. (1998) Etoposide: four decades of development of a topoisomerase II inhibitor. *Eur. J. Cancer* 34: 1514–1521.

Hayashi, K., Narutaki, K., Nagaoka, Y., Hayashi, T. and Uesato, S. (2010) Therapeutic effect of arctiin and arctigenin in immunocompetent and immunocompromised mice infected with influenza A virus. *Biol. Pharm. Bull.* 33: 1199–1205.

Hegg, E.L. and Que, L., Jr. (1997) The 2-His-1-carboxylate facial triad an emerging structural motif in mononuclear non-heme iron (II) enzymes. *Eur. J. Biochem.* 250: 625–629.

Hendrawati, O., Woerdenbag, H.J., Hille, J., Quax, W.J. and Kayser, O. (2011) Seasonal variations in the deoxypodophyllotoxin content and yield of *Anthriscus sylvestris* L. (Hoffm.) grown in the field and under controlled conditions. *J. Agric. Food Chem.* 59: 8132–8139.

Hirose, N., Inoue, T., Nishihara, K., Sugano, M., Akimoto, K., Shimizu, S., et al. (1991) Inhibition of cholesterol absorption and synthesis in rats by sesamin. *J. Lipid Res.* 32: 629–638.

Hyam, S.R., Lee, I.-A., Gu, W., Kim, K.-A., Jeong, -J.-J., Jang, S.-E., et al. (2013) Arctigenin ameliorates inflammation in vitro and in vivo by inhibiting the PI3K/AKT pathway and polarizing M1 macrophages to M2-like macrophages. *Eur. J. Pharmacol.* 708: 21–29.

Jang, Y.P., Kim, S.R., Choi, Y.H., Kim, J., Kim, S.G., Markelonis, G.J., et al. (2002) Arctigenin protects cultured cortical neurons from glutamate-induced neurodegeneration by binding to kainate receptor. *J. Neurosci. Res.* 68: 233–240.

Jin, S.-H., Lee, H., Shin, Y., Kim, J.-H. and Rhee, S. (2020) Crystal structure of the indole-3-acetic acid-catabolizing enzyme DAO1 from *Arabidopsis thaliana*. *J. Struct. Biol.* 212: 107632.

Jumper, J., Evans, R., Pritzel, A., Green, T., Figurnov, M., Ronneberger, O., et al. (2021) Highly accurate protein structure prediction with AlphaFold. *Nature* 596: 583–589.

Kawai, Y., Ono, E. and Mizutani, M. (2014) Evolution and diversity of the 2-oxoglutarate-dependent dioxygenase superfamily in plants. *Plant J.* 78: 328–343.

Kim, C.Y., Mitchell, A.J., Glinkerman, C.M., Li, F.S., Pluskal, T. and Weng, J.K. (2020) The chloroalkaloid (−)-acutumine is biosynthesized via a Fe(II)- and 2-oxoglutarate-dependent halogenase in Menispermaceae plants. *Nat. Commun.* 11: 1867.

Downloaded from https://academic.oup.com/pcp/article/64/12/1436/7329445 by guest on 22 May 2025

Kliebenstein, D.J., Lambrix, V.M., Reichelt, M., Gershenzon, J. and Mitchell-Olds, T. (2001) Gene duplication in the diversification of secondary metabolism: tandem 2-oxoglutarate–dependent dioxygenases control glucosinolate biosynthesis in *Arabidopsis*. *Plant Cell* 13: 681–693.

Kollipara, R., Ekhlassi, E., Downing, C., Guidry, J., Lee, M. and Tyring, S.K. (2015) Advancements in pharmacotherapy for noncancerous manifestations of HPV. *J. Clin. Med.* 4: 832–846.

Lam, P.Y., Lui, A.C., Wang, L., Liu, H., Umezawa, T., Tobimatsu, Y., et al. (2021) Tricin biosynthesis and bioengineering. *Fron. Plant Sci.* 12: 733198.

Lata, H., Mizuno, C.S. and Moraes, R.M. (2009) The role of biotechnology in the production of the anticancer compound podophyllotox. *In* Protocols for In Vitro Cultures and Secondary Metabolite Analysis of Aromatic and Medicinal Plants. Edited by Jain, S.M. and Saxena, P.K. pp. 387–402. Humana Press, New York, USA.

Lau, W. and Sattely, E.S. (2015) Six enzymes from mayapple that complete the biosynthetic pathway to the etoposide aglycone. *Science* 349: 1224–1228.

Li, H. and Cimino, S.K. (2020) Clinical impact of the etoposide injection shortage. *J. Oncol. Pharm. Pract.* 26: 187–192.

Liu, C.-M., Zheng, G.-H., Ming, Q.-L., Chao, C. and Sun, J.-M. (2013) Sesamin protects mouse liver against nickel-induced oxidative DNA damage and apoptosis by the PI3K-Akt pathway. *J. Agric. Food Chem.* 61: 1146–1154.

Liu, T., Huang, Y., Jiang, L., Dong, C., Gou, Y. and Lian, J. (2021) Efficient production of vindoline from tabersonine by metabolically engineered *Saccharomyces cerevisiae*. *Commun. Biol.* 4: 1–9.

MacRae, W.D. and Towers, G.H.N. (1984) Biological activities of lignans. *Phytochemistry* 23: 1207–1220.

Majdalawieh, A.F., Yousef, S.M., Abu-Yousef, I.A. and Nasrallah, G.K. (2022) Immunomodulatory and anti-inflammatory effects of sesamin: mechanisms of action and future directions. *Crit. Rev. Food Sci. Nutr.* 62: 5081–5112.

Marques, J.V., Kim, K.-W., Lee, C., Costa, M.A., May, G.D., Crow, J.A., et al. (2013) Next generation sequencing in predicting gene function in podophyllotoxin biosynthesis. *J. Biol. Chem.* 288: 466–479.

Martinez, S. and Hausinger, R.P. (2015) Catalytic mechanisms of Fe(II)- and 2-oxoglutarate-dependent oxygenases. *J. Biol. Chem.* 290: 20702–20711.

Motyka, S., Jafernik, K., Ekiert, H., Sharifi-Rad, J., Calina, D., Al-Omari, B., et al. (2023) Podophyllotoxin and its derivatives: potential anticancer agents of natural origin in cancer chemotherapy. *Biomed. Pharmacother.* 158: 114145.

Nakayasu, M., Akiyama, R., Kobayashi, M., Lee, H.J., Kawasaki, T., Watanabe, B., et al. (2020) Identification of α-tomatine 23-hydroxylase involved in the detoxification of a bitter glycoalkaloid. *Plant Cell Physiol.* 61: 21–28.

Orčić, D., Berezni, S., Skoric, D. and Mimica-Dukic, N. (2021) Comprehensive study of *Anthriscus sylvestris* lignans. *Phytochemistry* 192: 112958.

Phillips, K. and de la Peña, A.H. (2011) The combined use of the thermofluor assay and thermoQ analytical software for the determination of protein stability and buffer optimization as an aid in protein crystallization. *Curr. Protoc. Mol. Biol.* 94: 10.28.11–10.28.15.

Ragamustari, S.K., Nakatsubo, T., Hattori, T., Ono, E., Kitamura, Y., Suzuki, S., et al. (2013) A novel *O*-methyltransferase involved in the first methylation step of yatein biosynthesis from matairesinol in *Anthriscus sylvestris*. *Plant Biotechnol.* 30: 375–384.

Ragamustari, S.K., Yamamura, M., Ono, E., Hattori, T., Suzuki, S., Suzuki, H., et al. (2014) Substrate-enantiomer selectivity of matairesinol *O*-methyltransferases. *Plant Biotechnol.* 31: 257–267.

Sackett, D.L. (1993) Podophyllotoxin, steganacin and combretastatin: natural products that bind at the colchicine site of tubulin. *Pharmacol. Ther.* 59: 163–228.

Saitoh, T., Kuramochi, K., Imai, T., Takata, K.-I., Takehara, M., Kobayashi, S., et al. (2008) Podophyllotoxin directly binds a hinge domain in E2 of HPV and inhibits an E2/E7 interaction in vitro. *Bioorg. Med. Chem.* 16: 5815–5825.

Saitou, N. and Nei, M. (1987) The neighbor-joining method: a new method for reconstructing phylogenetic trees. *Mol. Biol. Evol.* 4: 406–425.

Sakakibara, N., Suzuki, S., Umezawa, T. and Shimada, M. (2003) Biosynthesis of yatein in *Anthriscus sylvestris*. *Org. Biomol. Chem.* 1: 2474–2485.

Saleem, M., Kim, H.J., Ali, M.S. and Lee, Y.S. (2005) An update on bioactive plant lignans. *Nat. Prod. Rep.* 22: 696–716.

Satake, H., Koyama, T., Bahabadi, S.E., Matsumoto, E., Ono, E. and Murata, J. (2015) Essences in metabolic engineering of lignan biosynthesis. *Metabolites* 5: 270–290.

Srinivasan, P. and Smolke, C.D. (2020) Biosynthesis of medicinal tropane alkaloids in yeast. *Nature* 585: 614–619.

Stähelin, H.F. and von Wartburg, A. (1991) The chemical and biological route from podophyllotoxin glucoside to etoposide: ninth Cain memorial Award lecture. *Cancer Res.* 51: 5–15.

Suzuki, S. and Umezawa, T. (2007) Biosynthesis of lignans and norlignans. *J. Wood Sci.* 53: 273–284.

Takehara, S., Sakuraba, S., Mikami, B., Yoshida, H., Yoshimura, H., Itoh, A., et al. (2020) A common allosteric mechanism regulates homeostatic inactivation of auxin and gibberellin. *Nat. Commum.* 11: 1–10.

Tamura, K., Stecher, G., Kumar, S. and Battistuzzi, F.U. (2021) MEGA11: molecular evolutionary genetics analysis version 11. *Mol. Biol. Evol.* 38: 3022–3027.

Tang, H., Wu, M.-H., Lin, H.-Y., Han, M.-R., Tu, Y.-H., Yang, Z.-J., et al. (2022) Mechanistic analysis of carbon–carbon bond formation by deoxypodophyllotoxin synthase. *Proc. Natl. Acad. Sci. U.S.A.* 119: e2113770119.

Umezawa, T. (2003a) Diversity in lignan biosynthesis. *Phytochem. Rev.* 2: 371–390.

Umezawa, T. (2003b) Phylogenetic distribution of lignan producing plants. *Wood Res.* 90: 27–110.

Umezawa, T., Yamamura, M., Ono, E., Shiraishi, A. and Ragamustari, S.K. (2019) Recent advances in lignan OMT studies. *Mokuzai Gakkaishi.* 65: 1–12.

Van Uden, W., Bos, J.A., Boeke, G.M., Woerdenbag, H.J. and Pras, N. (1997) The large-scale isolation of deoxypodophyllotoxin from rhizomes of *Anthriscus sylvestris* followed by its bioconversion into 5-methoxypodophyllotoxin β-D-glucoside by cell cultures of *Linum flavum*. *J. Nat. Prod.* 60: 401–403.

Weng, J.K. (2014) The evolutionary paths towards complexity: a metabolic perspective. *New Phytol.* 201: 1141–1149.

Wittig, I., Braun, H.-P. and Schägger, H. (2006) Blue native PAGE. *Nat. Protoc.* 1: 418–428.

Yamamura, M., Kumatani, M., Shiraishi, A., Matsuura, Y., Kobayashi, K., Suzuki, A., et al. (2023) Two *O*-Methyltransferases from phylogenetically unrelated cow parsley (*Anthriscus sylvestris*) and hinoki-asunaro (*Thujopsis dolabrata* var. hondae) as a signature of lineage-specific evolution in lignan biosynthesis. *Plant Cell Physiol.* 64: 124–147.

Záleśák, F., Bon, D.J.-Y.D. and Pospíšil, J. (2019) Lignans and neolignans: plant secondary metabolites as a reservoir of biologically active substances. *Pharmacol. Res.* 146: 104284.

Downloaded from https://academic.oup.com/pcp/article/64/12/1436/7329445 by guest on 22 May 2025